Coupled-States Statistical Investigation of Vibrational and Rotational Relaxation of OH($^2\Pi$) by Collisions with Atomic Hydrogen†

Sule Atahan and Millard H. Alexander*

Department of Chemistry and Biochemistry, University of Maryland, College Park, Maryland 20742

Received: October 13, 2005; In Final Form: November 30, 2005

We report state-to-state cross sections and thermal rate constants for vibrational and rotational relaxation of OH($^2\Pi$) by collision with H atoms. The cross sections are calculated by the coupled-states (CS) statistical method including the full open-shell character of the OH + H system. Four potential energy surfaces (PESs) (^{1,3}A′ and ^{1,3}A″) describe the interaction of OH($X^2\Pi$) with H atoms. Of these, three are repulsive, and one (^{1}A′) correlates with the deep H_2O well. Consequently, rotationally and ro-vibrationally inelastic scattering of OH in collisions with H can occur by scattering on the repulsive PESs, in a manner similar to the inelastic scattering of OH by noble gas atoms, or by collisions which enter the H_2O well and then reemerge. At 300 K, we predict large ($\approx 1 \times 10^{-10}$ cm^3 molecule^{-1} s^{-1}) vibrational relaxation rates out of both $v = 2$ and $v = 1$, comparable to earlier experimental observations. This anomalously fast relaxation results from capture into the H_2O complex. There exists a significant propensity toward formation of OH in the Π(A′) Λ-doublet level. We also report state-resolved cross sections and rate constants for rotational excitation within the OH $v = 0$ manifold. Collisional excitation from the F_1 to the F_2 spin−orbit manifold leads to an inverted Λ-doublet population.

1. Introduction

The hydroxyl radical is an important species in combustion, astrophysics and atmospheric chemistry. In the Earth's atmosphere, vibrationally activated OH is produced by the following reactions:[1,2]

$$H + O_3 \rightarrow OH(v \leq 9) + O_2 \qquad \text{(mesopause)} \qquad (1)$$

$$O(^1D) + H_2O \rightarrow 2OH(v \leq 3) \qquad \text{(stratosphere and troposphere)} \qquad (2)$$

To model the chemistry of the OH radical, after formation, it is essential to understand the rates of OH vibrational relaxation.[3] The collisional relaxation of OH in its ground ($X^2\Pi$) electronic state with a number of atomic[4,5] as well as diatomic molecules,[4−14] has been subject of many, mostly experimental, studies.

Vibrational relaxation of free radicals has been less well studied than that of closed-shell systems. Smith has argued[7] that the rates of vibrational relaxation in potentially reactive encounters are much higher than for nonreactive encounters. In particular, for radical−radical collisions, there is often a barrierless access to a deep well. Within the ensuing complex, the statistical scrambling of the various degrees of freedom should allow access to all energetically allowed rovibrational states.[7,15] The adiabatic channel model[16−18] can be used to simulate this statistical scrambling of energy. In addition, collisions of open-shell species are often governed by multiple potential energy surfaces, which are degenerate asymptotically.[19,20] In this case crossing between attractive and repulsive adiabats corresponding to multiple potential energy surfaces should facilitate vibrational relaxation.[19]

Smith has argued[7] that the formation of the collision complex is the rate determining step so that the rate of relaxation will not depend significantly on the degree of vibrational excitation of the reactants. On the other hand, because the topology of the attractive potential energy surface will depend on the bond distance of the diatomic moiety, it may well be that access to the complex does depend on the degree of vibrational excitation.

Recent developments in statistical theories of reaction dynamics by Manolopoulos and co-workers[21−23] now allow one to go beyond earlier adiabatic channel[16−18] methods by carrying out fully quantum scattering calculations which include all couplings prior to capture into the complex. A time-dependent version of this method was subsequently developed by Guo and coworkers.[24,25] These quantum capture calculations have been successfully applied to insertion reactions[21,22,24,25] which traverse a deep well. More recently, Alexander, Rackham and Manolopoulos[23] modified and extended the theory to include nonadiabatic couplings between asymptotically degenerate electronic states.

In this paper, we use the same quantum capture method to investigate the inelastic scattering dynamics of the OH radicals in collision with H. Although collision of OH with H is not an important process in the mesosphere, this simple system can serve as a prototype for the study of the effect of complex formation on vibrational relaxation. One particular goal of the present study will be the investigation of the relative efficiency of vibrational relaxation during collisions that do not penetrate the complex as compared to vibrational relaxation by redistribution of energy within the complex.

To the best of our knowledge, there have appeared only two reports of measurements of vibrational relaxation rates of OH due to collisions with H atoms. In a study of the reaction of NO_2 with atomic hydrogen, Spencer and Glass[15] reported the relaxation rates of OH in $v = 2$ and $v = 1$ with collisions with

† Part of the special issue "John C. Light Festschrift".

10.1021/jp055860m CCC: $33.50
Published on Web 01/11/2006

TABLE 1: Summary of Calculated and Measured Rate Constants for the Vibrational Relaxation of OH($v = 1, 2$)

	$k_{v\to v'}/10^{-10}$ cm^3 molecule^{-1} s^{-1}			
T/K	$2 \to 0$	$2 \to 1$	$2 \to 1 + 0$	$1 \to 0$
50	1.259[a]	0.842[a]	2.099[a]	2.013[a]
100	1.209[a]	0.788[a]	1.996[a]	1.915[a]
300	1.043[a]	0.654[a]	1.697[a]	1.600[a]
	1.43[b]	0.753[b]	2.18[b]	2.1[b]
			3.3[c]	2.7[c]
				1.5 ± 0.4[d]
				1.4 ± 0.12[e]

[a] This work. [b] Theoretical; ref 16. [c] Experimental; ref 15. [d] Experimental; ref 26, derived from an experiment in which H_2O was excited to the $|13\rangle$ vibrational level. [e] Experimental; ref 26, derived from an experiment in which H_2O was excited to the $|12\rangle$ vibrational level.

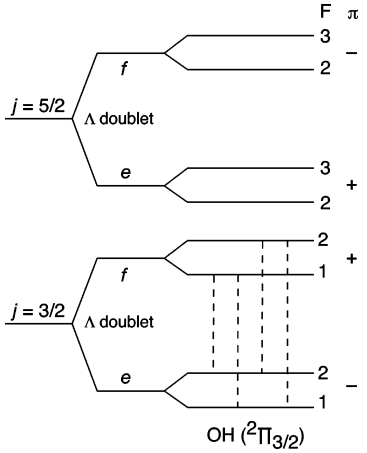

Figure 1. Schematic diagram of the lowest two rotational levels in the lower F_1 ($^2\Pi_{3/2}$) spin−orbit manifold of OH. The levels are labeled with the total angular momentum exclusive of the nuclear spin, *j*, the *e*/*f* symmetry (Λ-doublet) labels (refs 48 and 49), the total angular momentum including the nuclear spin, *F*, and the parity π. This figure is adapted from Figure 1 of ref 37. The Λ-doublet and hyperfine splittings are greatly exaggerated for clarity. The four OH maser transitions[30] at 1612, 1665, 1667 and 1720 MHz are shown by the dashed vertical lines.

H (see Table 1). More recent measurements have been reported by Smith et al.[26] These authors determined the rate of reaction and relaxation of H_2O by collisions with H and H_2O, and report the relaxation rate of OH ($v = 1 \to 0$) to be $\approx 1.5 \times 10^{-10}$ cm^3 molecule^{-1} s^{-1} (see Table 1), which corresponds to a thermally averaged cross-section of ≈ 5.5 Å^2. The only theoretical determination of OH(v) + H relaxation rates is an early study by Quack and Troe.[16]

In addition to its importance in atmospheric chemistry, the OH radical has drawn considerable attention because of the importance of the OH maser as a tool for acquiring insights into the physical processes occurring within interstellar clouds.[27−29] The presence of the OH molecule in interstellar clouds is identified by its four radio emission lines at frequencies of 1612, 1665, 1667 and 1720 MHz.[30] These are attributed to maser emission from inverted populations in the Λ-doublet levels of the OH molecule. Figure 1 shows a diagram of the lowest Λ-doublet with the hyperfine-structure responsible for the indicated emissions.

There have been numerous suggestions about the possible pump mechanisms responsible for the Λ-doublet level population inversion. One possible cause involves inelastic collisions of OH with H and H_2, followed by radiative decay.[31−34] Suppose that collisional excitation to higher rotational levels were to favor, preferentially, the upper Λ-doublet. Subsequent radiative

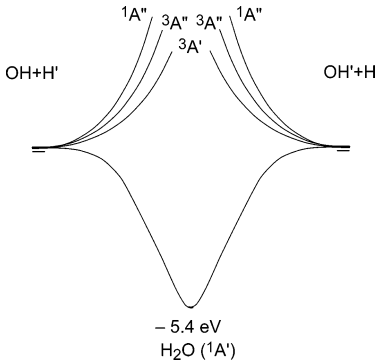

Figure 2. Schematic illustration of the OH + H′ ↔ OH′ + H potential energy surfaces. The O(^{1}D) + H_2 arrangement (not shown) lies 1.89 eV higher than the OH + H asymptotes.

transitions to the ground rotational level will change the parity but conserve the Λ-doublet label. As a consequence, the upper Λ-doublet of the ground rotational level will be preferentially populated.

There have appeared a number of sophisticated studies of rotationally inelastic collisions of OH with H_2.[35−40] The theoretical simulation of collisions of OH with H atoms is further complicated by the presence of the deep H_2O well, as well as by the necessity of dealing with the open-shell character of both OH($^2\Pi$) and H(^{2}S), with nonzero electronic orbital angular momentum, electronic spin, and nuclear spin. An early, approximate study by Bertojo and co-workers[33] supported the pumping mechanism discussed in the previous paragraph.

To the best of our knowledge, the first rigorous theoretical treatment that retained the open-shell character of both the OH radical and the H atom was presented by Shapiro and Kaplan.[41] These authors calculated state-to-state rate constants for transitions between and within the $j = {}^3/_2$ and $j = {}^5/_2$ rotational levels in the (lower) $^2\Pi_{3/2}$ spin−orbit manifold. They predicted steady-state level distributions by means of a simple cloud model which included their rate constants, stimulated and spontaneous emission probabilities and the 2.7 K background radiation. Their model predicted that OH + H inelastic collisions could play an important role in producing the observed Λ-doublet inversions.

As shown schematically in Figure 2, a complete description of the interaction of OH($X^2\Pi$) with H(^{2}S) requires four potential energy surfaces (^{1,3}A′ and ^{1,3}A″).[23] Of these, three are repulsive, and one (^{1}A′) correlates with the deep H_2O (X^1A′) well. Consequently, rotational and ro-vibrational relaxation of OH in collisions with H can occur either by scattering on the repulsive PESs, in a manner similar to the inelastic scattering of OH by noble gas atoms, or by collisions which enter the H_2O well and then reemerge (the O + H_2 channel is energetically closed at collision energies below 1.8 eV).

The goal of this Article will be to use the close-coupled statistical method,[21,22] as extended by Alexander,[23] in the determination of cross sections for rotational and ro-vibrational relaxation of OH($X^2\prod$) in collisions with H. Section 2 summarizes the relevant details of the method, the Hamiltonian, PESs and the calculations. In section 3, we present cross sections and thermal rate constants for $v = 1, 2 \to v = 0$ rovibrational relaxation and for rotationally inelastic collisions within the $v = 0$ level. A brief summary concludes the paper.

2. Theory and Computational Methods

Even at energies below the O(^{1}D) + H_2 channel, the title reaction samples the product valley of the O(^{1}D) + H_2 → OH + H insertion reaction. The exact quantum treatment of

insertion reactions involving deep wells is complicated by the necessity of using large basis sets to describe all the bound and quasi-bound states accessed in these wells.[42] Recently, Rackham and co-workers successfully unified[21−23] the venerable statistical model, proposed initially by Pechukas and Light, as well as by Nikitin,[43,44] with the close-coupled capture theory of Clary and Henshaw.[45] In the close-coupled statistical method of Manolopoulos and co-workers all coupling within the various arrangement channels is included, but separately for each arrangement, in the determination of exact capture probabilities. These are then combined, following the usual statistical prescription,[43,44,46] to yield the following expression for the probability of collisional transfer from state n to state n', due to capture and then subsequent decay of the metastable complex:

$$P_{nn'}^{\text{complex}} = \frac{P_n P_{n'}}{\sum_{n''} P_{n''}} \tag{3}$$

Here P_n and $P_{n'}$ are the respective capture probabilities for states n and n'. In the studies of chemical reactions, which were the object of the earlier articles,[21−23] P_n and $P_{n'}$ refer to separate arrangements. Here, as will be discussed in more detail below, these two capture probabilities can refer either to the same or to different arrangements. The sum in the denominator runs over all energetically accessible states in any arrangement. Application of the statistical model is based on the assumption that the complex spends enough time in the well to scramble all direct connection between reactants and products.

Rackham, Manolopoulos and co-workers used a time-independent formalism to determine the capture probabilies (and, consequently, cross sections). A conceptually similar, time-dependent method has been described by Guo.[24,25] In comparison with exact quantum scattering calculations on the $O(^1D) + H_2 \rightarrow OH + H$ reaction,[42] in which a single potential energy surface was used, the close-coupled, statistical model, in both the full close-coupled and the computationally simpler, coupled-states approximation,[21,22] yielded excellent agreement for both integral and differential state-resolved cross sections.

As mentioned in the Introduction, Alexander, Rackham and Manolopoulos (ARM)[23] have extended the close-coupled, statistical model to include the electronic degrees of freedom (orbital and spin angular momenta) of the OH and H fragments. This necessitates inclusion of the four potential energy surfaces ($^{1,3}A'$ and $^{1,3}A''$, shown in Figure 2) that correlate with $OH(X^2\Pi) + H(^2S)$. Although Honvault and Launay[42] have reported fully quantum reactive scattering calculations for the $O(^1D) + H_2$ reaction, these were limited to the approximation that only a single potential energy surface was involved. Because the full description of the electronic degrees of freedom in the product arrangement necessitates inclusion of four potential energy surfaces, full multi-potential-energy-surface scattering calculations on collisions of OH with H would be extremely demanding, from a computational standpoint.

Here we apply the close-coupled statistical method to the inelastic scattering of OH in collisions with H. Experimentally it would be difficult (if not impossible) to distinguish the separate contribution to inelastic scattering from collisions that are absorbed into the complex ($P_{n'n}^{\text{complex}}$, eq 3) from the contribution to relaxation that occurs by scattering on the repulsive potential energy surfaces ($P_{n'n}^{\text{direct}}$), in a manner similar to the inelastic scattering of OH in collisions with noble gas atoms. As will be discussed in more detail below, the latter probability is calculated from the **S**-matrix, just as in conventional inelastic scattering calculations.

In fact, vibrational relaxation can occur by this direct (noncapture) scattering in the initial arrangement

$$OH(v, j) + H' \rightarrow OH(v', j') + H' \tag{4}$$

by decay of the complex back to the initial arrangement

$$OH(v, j) + H' \rightarrow HOH'^{\ddagger} \rightarrow OH(v', j') + H' \tag{5}$$

or by decay of the complex accompanied by hydrogen atom exchange

$$OH(v, j) + H' \rightarrow HOH'^{\ddagger} \rightarrow OH'(v', j') + H \tag{6}$$

Let us designate by $P_{n'}^a$ and $P_{n'}^b$ the capture probabilities for the $OH(v', j') + H'$ and $OH'(v', j') + H$ arrangements, where the single index n' stands for v', j'. The total vibrational deactivation probability for processes (4)−(6) is given by the sum of the probabilities for complex-mediated $OH(v, j) \rightarrow OH(v', j')$ and $OH(v, j) \rightarrow OH'(v', j')$ relaxation, plus the probability for direct $OH(v, j) \rightarrow OH(v', j')$ relaxation through collisions which do not enter the complex. In other words

$$P_{nn'}^{\text{tot}} = \frac{P_n^a P_{n'}^a + P_n^a P_{n'}^b}{\sum_{n''} P_{n''}^a + P_{n''}^b} + P_{nn'}^{\text{direct}} = \frac{P_n^a P_{n'}^a}{\sum_{n''} P_{n''}^{\text{a}}} + P_{nn'}^{\text{direct}} \tag{7}$$

The simplification made in eq 7 exploits the fact that the $OH(v', j') + H'$ and $OH'(v', j') + H$ capture probabilities, $P_{n'}^a$ and $P_{n'}^b$, are identical.

2.1. Hamiltonian and Basis. The quantum mechanical description of triatomic collisions involving open-shell molecules is similar to that of closed-shell molecules, in that the total wave function is expanded in a set of products of functions describing the internal motion of the diatomic moeity. The expansion coefficients are a function of the Jacobi separation vector. In the case of an open-shell molecule, the Hamiltonian for the internal motion includes both the usual vibrational and rotational motion as well as spin−orbit and Λ-doubling terms.[47] The present study is based on the framework presented by ARM.[23] As mentioned earlier, we will briefly summarize the underlying theory and highlight only the differences between this and the previous study of multiplet branching in the $O(^1D) + H_2 \rightarrow OH + H$ reaction.

The capture probabilities are determined according to the Hamiltonian,

$$\mathbf{H}_{OH+H}(\vec{R}, \vec{r}, \vec{q}) = \mathbf{T}_n(\vec{R}) + \mathbf{V}_{\text{el}}(\vec{q}; \vec{R}, \vec{r}) + \mathbf{H}_{\text{mol,OH}}(\vec{q}; \vec{r}) \tag{8}$$

Here $\vec{R}$ and $\vec{r}$ are the Jacobi coordinates for a particular arrangement, and $\vec{q}$ represents the electronic coordinates. The first term $\mathbf{T}_n$ represents the kinetic energy of the relative atom−diatom motion:

$$\mathbf{T}_n = -\frac{\hbar^2}{2\mu R^2}\frac{\partial}{\partial R}R^2\frac{\partial}{\partial R} + \frac{L_{\text{op}}{}^2}{2\mu R^2} \tag{9}$$

The second term, $\mathbf{V}_{\text{el}}$, is the electrostatic interaction, and the third term, $\mathbf{H}_{\text{mol}}$, is the OH molecular Hamiltonian.

TABLE 2: Spectroscopic Constants for OH (cm^{-1})[a]

p_v	$0.235 - 0.006v$
q_v	$-0.0391 + 0.0018v$
A_v	$-139.21 - 0.275v$
B_v	$18.910 - 0.7242(v + 1/2)$

[a] Reference 61.

The overall wave function for the OH−H system is expanded in the basis

$$\langle \hat{R}, \vec{r}\,|JMKvjk\lambda\sigma\sigma_h\rangle = \frac{1}{r}\hat{D}^{J*}_{MK}(\Omega)\hat{d}^{j}_{k\omega}(\gamma)\,\chi_{vj}(r)|\lambda\sigma\rangle|\sigma_h\rangle \quad (10)$$

Here, J is the total angular momentum with projection K along OH−H vector $\vec{R}$ and M along the space-frame z-axis. The quantum number j designates the rotational angular momentum of OH diatom, with projection k along $\vec{R}$ and with projection ω along $\vec{r}$. Also, $\hat{D}^{J*}_{MK}(\Omega) = ([2j+1]/8\pi^2)^{1/2}D^{J*}_{MK}(\Omega)$ is the normalized Wigner rotation matrix element, where Ω denotes the three Euler angles that relate the space-fixed and body-fixed frames. Further, χ is the OH vibrational wave function. The first ket, $|\lambda\sigma\rangle$, designates the electronic wave function of the OH molecule, where λ and σ are the projections of the electronic orbital and spin angular momenta along $\vec{r}$ and $\omega = \lambda + \sigma$. The second ket, $|\sigma_h\rangle$, represents the electronic wave function of the H atom, where σ_h is the projection of the H-atom spin along $\vec{R}$. The projection of the total angular momenta J along $\vec{R}$ is $K = k + \sigma_h$.

The determination of the matrix elements of $\mathbf{V}_{el}$ and $\mathbf{H}_{mol}$ in the basis defined by eq 10 is presented in detail in ref 23. As discussed in ref 23, the matrix elements of $\mathbf{V}_{el}$ can be evaluated in terms of the four OHH potential energy surfaces, shown schematically in Figure 2. As reported by ARM,[23] the potential energy surfaces were calculated by internally contracted, multireference, configuration-interaction calculations.

The vibration−rotation-fine-structure levels of the free OH radical are obtained by diagonalizing $\mathbf{H}_{mol}$ in a parity-adapted, Hund's case (a) basis defined by

$$|vjm\omega\epsilon\rangle = \frac{1}{\sqrt{2}}[|jm\omega\rangle|\lambda\sigma\rangle + \epsilon|jm, -\omega\rangle|-\lambda, -\sigma\rangle]|v\rangle \quad (11)$$

where ω is assumed to be positive and can take on the values $^1/_2$ or $^3/_2$, and the symmetry (Λ-doublet) index $\epsilon = \pm 1$. In this basis, the matrix elements of $\mathbf{H}_{mol}$ are diagonal in j, m, v and ϵ and given by

$$\left\langle \omega = \frac{1}{2}\epsilon\middle|H_{mol}\middle|\omega = \frac{1}{2}\epsilon\right\rangle = E_v - A_v/2 + (j+1/2)^2B_v + [1-\epsilon(j+1/2)]p_v/2 + [1-\epsilon(j+1/2)]^2q_v/2 \quad (12)$$

$$\left\langle \omega = \frac{1}{2}\epsilon\middle|H_{mol}\middle|\omega = \frac{3}{2}\epsilon\right\rangle = -\frac{1}{4}[(j+1/2)^2-1]^{1/2}\{4B_v + p_v + 2[1-\epsilon(j+1/2)]q_v\} \quad (13)$$

$$\left\langle \omega = \frac{3}{2}\epsilon\middle|H_{mol}\middle|\omega = \frac{3}{2}\epsilon\right\rangle = E_v + A_v/2 + [(j+1/2)^2-2]B_v + [(j+1/2)^2-1]q_v/2 \quad (14)$$

The pertinent spectroscopic constants which define these matrix elements are given in Table 2. In particular, B_v is the rotational constant, A_v is the spin−orbit constant and p_v and q_v are the Λ-doubling constants.

As illustrated schematically in Figure 3, there exist two rotational ladders, F_1 and F_2, separated by the spin−orbit splitting. In addition, for each value of the OH rotational angular momentum, there exist two Λ-doublet levels, separated only by a fraction of a wavenumber. In intermediate and case (b) Hund's coupling, the two Λ-doublet levels can be distinguished by the reflection symmetry of the spatial part of the electronic wave function in the plane of rotation of the diatomic.[48] In the lower (F_1) spin−orbit manifold, the e-labeled Λ-doublet levels[49] have, in the high-j limit, nominal A′ reflection symmetry, whereas the f-labeled levels have nominal A″ reflection symmetry.[48,50] The association of reflection symmetry with the e/f label is reversed in the upper (F_2) spin−orbit manifold. Note that the A′ Λ-doublet levels are lower in energy in the F_1 spin−orbit manifold, but higher in energy in the F_2 spin−orbit manifold. This situation is reversed in the F_2 spin−orbit manifold for levels with $j \geq {}^9/_2$. Thus, except for the F_2 levels with $^1/_2 \leq j \leq {}^7/_2$, the lower of the two Λ-doublet levels always corresponds to nominal A′ reflection symmetry.

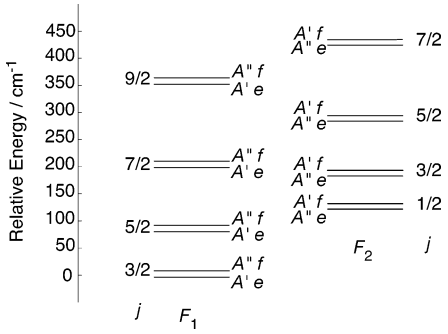

Figure 3. Relative spacings of the lower spin-rotation levels of OH($X^2\Pi$). For clarity, the magnitude of the Λ-doublet splitting has been greatly exaggerated in the figure.

2.2. Scattering Calculations. The wave function is expanded in the basis of eq 10. Premultiplication by individual members of the basis, integration over all the electronic and nuclear coordinates except R and evaluation of the resulting matrix elements following the preceding subsection gives rise to the set of close-coupled equations familiar in inelastic scattering. These equations are solved subject to modified boundary conditions that allow for a nonvanishing incoming wave for each adiabatic state which is not energetically closed at the capture radius R_c.[21,22] The resulting **S**-matrix is obtained by outward propagation, similar to the procedure in the conventional treatment of inelastic scattering.[51−53] The **S**-matrix, although symmetric, is, however, no longer unitary because the capture boundary condition acts like a sink.

As discussed earlier,[21,22] the computationally more efficient coupled-states approximation can be used, wherein both the total angular momentum J and its projection K along $\vec{R}$ are conserved. At a given value of the total energy E and the quantum numbers J and K, the probability of capture for an OH + H′ collision in which the diatomic moiety is in initial state n is

$$P^{JK}_n(E) = 1 - \sum_{n'}|S^{JK}_{nn'}(E)|^2 = 1 - \sum_{n'} P_{nn'}{}^{JK,\mathrm{direct}} \quad (15)$$

Here the sum is over all energetically accessible states. In reality the single index n designates the set of quantum numbers $\{v, j, k, F_i, \epsilon, \sigma_h\}$. The transition probability for an inelastic $n \rightarrow n'$ transition, due to coupling before capture, which appears in eq 7, is given by

$$P^{JK,\mathrm{direct}}_{nn'} = |S^{JK}_{nn'}(E)|^2 \quad (16)$$

TABLE 3: Values of the Parameters Used in the Present Calculations

	R_c/au	j_{max}	E_{max}/eV[a]
OH($v = 1,2$)+H	3	30	1.6
OH($v = 0$)+H	3	25	0.9

[a] The zero energy corresponds to OH ($r = r_e$) + H.

If we insert, explicitly, all the relevant quantum numbers, then eq 7 becomes

$$P^J_{vjF_i\epsilon\sigma_h\to v'j'F_i'\epsilon'\sigma_h'}(E) = \sum_{KK'} \frac{P^{JK}_{vjF_i\epsilon\sigma_h}(E)\, P^{JK'}_{v'j'F_i'\epsilon'\sigma_h'}(E)}{\sum_{K''v''j''F_i''\epsilon''\sigma_h''} P^{JK''}_{v''j''F_i''\epsilon''\sigma_h''}(E)} + \sum_K |S^{JK}_{vjF_i\epsilon\sigma_h\to v'j'F_i'\epsilon'\sigma_h'}(E)|^2 \quad (17)$$

Within the coupled-states approximation the projection K of the total angular momentum along in the Jacobi vector of relative motion is conserved within each arrangement and is thus is a good quantum number. However, presumably, this is scrambled within the complex, so that there appear $K \to K'$ contributions in eq 17. Because only the initial arrangement is responsible for the direct contribution, K is conserved in the second summation on the right-hand-side of eq 17.

The corresponding integral state-to-state cross sections are given by

$$\sigma_{vjF_i\epsilon\sigma h\to v'j'F_i'\epsilon'\sigma_h'}(E) = \frac{\pi\hbar^2}{2\mu(E - E_{vjF_i})} \frac{1}{2j+1} \sum_J (2J+1) P^J_{vjF_i\epsilon\sigma_h\to v'j'F_i'\epsilon'\sigma_h'}(E) \quad (18)$$

where μ is the collision reduced mass. Because of the separation in eq 17 of the overall transition probability into a contribution from direct scattering and a complex-mediated contribution, we can similarly partition the contribution to the cross sections.

Scattering calculations were carried out at nearly 350 values of the total energy ranging from 0.2248 to 1.5 eV (1800−13 000 cm^{-1}). The zero of energy is taken to be H + OH($r = r_e$), so that this range of total energies corresponds roughly to collision energies ranging from ≈5−11 000 cm^{-1} in $v = 0$. The parameters that control the accuracy of the computed coupled-states statistical-model cross sections are the capture radius, R_c, and the size of the channel basis. The latter is controlled by two parameters E_{max} and j_{max}, so that all OH channels with $j > j_{max}$ or with internal energies $\epsilon_{vjF_i\epsilon} > E_{max}$ are excluded. The three parameters R_c, E_{max}, and j_{max} were adjusted to ensure the convergence of the capture probabilities P_c to within 0.5%; the adopted values are listed in Table 3. In particular, j_{max} was adjusted so that, at the highest value of the total energy, all open rotational levels as well as the lowest four energetically closed levels were included in the channel basis.

3. Results: Rovibrational Relaxation of OH

In our investigation of rovibrational relaxation, we shall assume that the initial Λ-doublet levels, which differ in energy by a mere fraction of a wavenumber, are equally populated. In this case the integral cross sections for production of a particular j', F_i' OH final state are obtained from eq 18 by summing over both final-state Λ-doublet levels and both H-atom spin-projection states, and averaging over the comparable initial states, to obtain

$$\sigma_{vF_ij\to v'F_i'j'} = \frac{1}{4} \sum_{\epsilon\epsilon'\sigma_h\sigma_h'} \sigma_{vF_ij\epsilon\sigma_h\to v'F_i'j'\epsilon'\sigma_h'} \quad (19)$$

By summing over all final states, we obtain the initially state-selected, total vibrational relaxation cross sections

$$\sigma_{vF_ij} = \sum_{v'<v,F_i'j'} \sigma_{vF_ij\to v'F_i'j'} \quad (20)$$

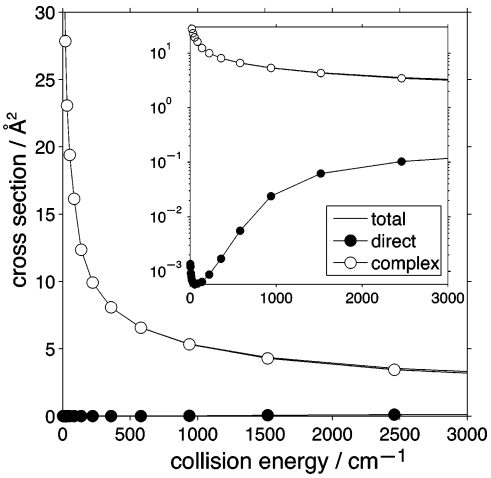

Figure 4. Direct and complex-mediated contributions to the Initially-state-selected total vibrational relaxation cross section for OH($v = 1$, F_1, $j = 3/2$) + H → OH($v = 0$) + H vibrational relaxation. The inset panel is a semilog plot to demonstrate the negligibly small size of the cross section for direct relaxation.

3.1. Direct As Compared to Complex-Mediated Relaxation. One of the primary goals of this investigation is to explore the relative importance of direct as compared to complex-mediated mechanisms for vibrational relaxation. Figure 4 shows the dependence on collision energy of the initially state-selected, total vibrational relaxation cross section (eq 20) for OH($v = 1$, F_1, $j = 3/2$). Here, as well as for the $v = 2 \to 0$ and $v = 2 \to 1$ processes (not shown), we found that vibrational relaxation is due overwhelmingly to collisions which enter the HOH′ complex and then reemerge. The very small contribution of direct scattering is even more insignificant at lower energy. [The magnitude of the small rise in the direct cross sections that appears at very low energies is within (or less than) our estimate of the precision of the scattering calculations.]

Figure 5 plots the percentage of the direct contribution for the lowest rotational level in both spin−orbit manifolds. The relative importance of direct scattering increases as a function of increasing collision energy but remains modest even at hyperthermal energies. For vibrational relaxation governed by a repulsive potential energy surface, simple SSH theory[54,55] predicts that the $v = 2 \to 1$ cross section will be roughly two times larger than the $1 \to 0$ cross section. This prediction applies well to the direct relaxation cross sections in Figure 5

Recently, Krems, Nordholm and co-workers have described[56,57] exact close-coupled calculations of vibrational relaxation cross sections for collisions of the closed-shell HF−Ar system. Their computed cross sections are on the order of 10^{-4}−10^{-3} Å^2 at collision energies below several thousand cm^{-1}. As might be expected, these values are very comparable to the direct vibrational relaxation cross sections shown in Figure 4.

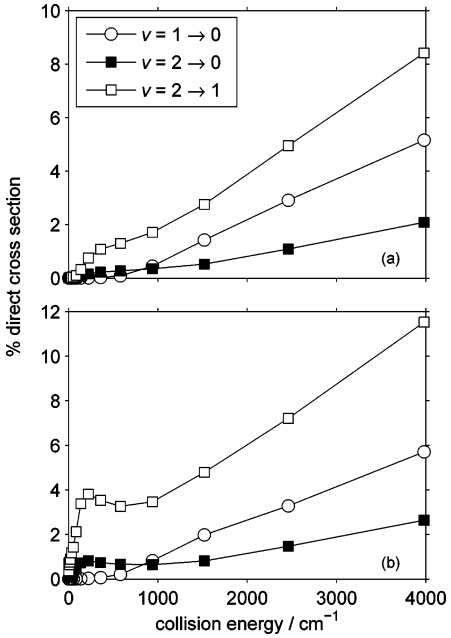

Figure 5. Relative percentage contribution of direct scattering to the vibrational relaxation cross sections as a function of collision energy for the lowest rotational levels of OH (panel a: $j = {}^3/_2$, F_1 and panel b: $j = {}^1/_2$, F_2).

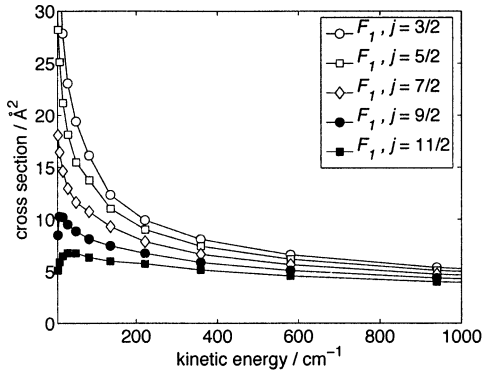

(a) $\mathrm{OH}(v = 1, F_1, j)+\mathrm{H}\rightarrow\mathrm{OH}(v = 0)+\mathrm{H}$

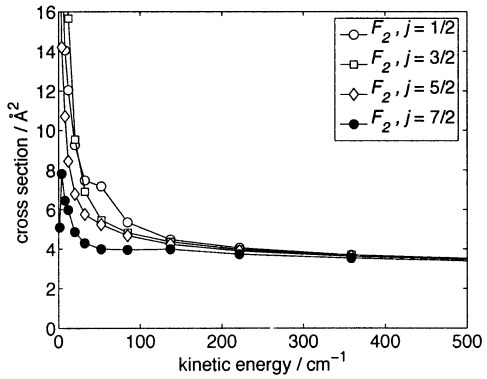

(b) $\mathrm{OH}(v = 1, F_2, j)+\mathrm{H}\rightarrow\mathrm{OH}(v = 0)+\mathrm{H}$

Figure 6. Initial rotational and spin-orbit resolved cross sections for OH($v = 1$, F_1/F_2, j) + H → OH($v = 0$) + H. Cross sections are calculated as described in eq 20.

3.2. Initial State Selected Relaxation Cross Sections. Figure 6 shows the initial state specific total cross sections calculated as described in eq 20 for relaxation of OH($v = 1$). As reported previously,[25,58,59] initial OH rotational excitation decreases the capture cross sections. The topology of the ^{1}A′ OH−H potential energy surface—strongly attractive only in bent geometries, but quite repulsive for both collinear geometries[23]—is responsible for this effect. The rotational motion averages out the OH−H potential, so that the incoming collision partners "see" less of the collision complex. Hence, the magnitude of the cross sections as well as the magnitude of the enhancement at low-energy decreases with increasing j. At higher energy, this effect disappears, because the collision occurs too quickly for the rotational averaging to occur.

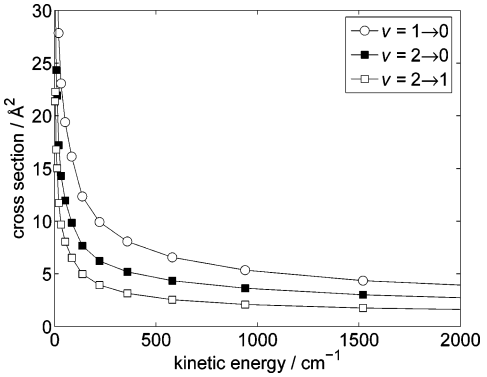

Figure 7. Initial state selected relaxation cross sections for OH(v, F_1, $j = {}^3/_2$) + H → OH(v') + H, for $v = 2 \rightarrow 1$, $2 \rightarrow 0$, and $1 \rightarrow 0$.

We observe a smaller relaxation cross section for the spin−orbit excited OH. However, the decrease in the vibrational relaxation cross section with increasing initial rotational angular momentum, discussed in the preceding paragraph, is apparent also in the upper spin−orbit manifold. Both these conclusions apply also to $v = 2 \rightarrow 1$, 0 relaxation.

Figure 7 compares the total vibrational relaxation cross sections for the $v = 2 \rightarrow 1$, $2 \rightarrow 0$, and $1 \rightarrow 0$ transitions, as a function of energy. We observe that the $v = 1 \rightarrow 0$ process has the largest cross section. If we neglect the small direct contribution to the relaxation in eq 17, then we see that the probabilities for the $v = 2 \rightarrow 1$, $2 \rightarrow 0$, and $1 \rightarrow 0$ transitions are given by

$$P_{v=1\rightarrow 0} = \frac{P_{v=1}P_{v=0}}{\sum P_{v=1} + \sum P_{v=0}} \tag{21}$$

$$P_{v=2\rightarrow 0} = \frac{P_{v=2}P_{v=0}}{\sum P_{v=2} + \sum P_{v=1} + \sum P_{v=0}} \tag{22}$$

and

$$P_{v=2\rightarrow 1} = \frac{P_{v=2}P_{v=1}}{\sum P_{v=2} + \sum P_{v=1} + \sum P_{v=0}} \tag{23}$$

Because the total energy is higher for collisions with OH initially in $v = 2$, the denominator is larger in the expressions for relaxation out of $v = 2$ (eqs 22 and 23). If we assume that the capture cross sections are roughly equal for $v = 2$, 1, and 0, then the $v = 1 \rightarrow 0$ relaxation probabilities will be larger.

Figure 8 shows the dependence on final rotational quantum number at a collision energy of 580.3 cm^{-1} for the $v = 2 \rightarrow 1$, $2 \rightarrow 0$, and $1 \rightarrow 0$ transitions. The $v = 2 \rightarrow 1$ and $v = 2 \rightarrow 0$ cross sections are virtually identical, except at high j', where only rotational levels in $v = 0$ are energetically accessible. Consequently, when summed over all final rotational levels, the $v = 2 \rightarrow 0$ cross sections will be larger than the $v = 2 \rightarrow 1$ cross sections at an identical collision energy, as seen in Figure 7.

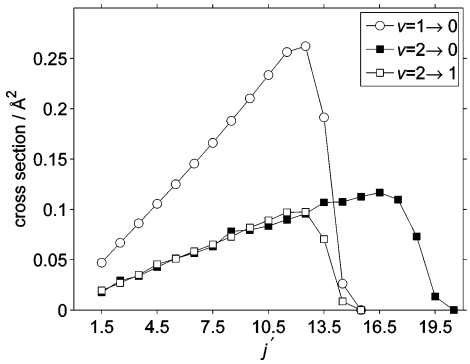

Figure 8. Comparison of the state-to-state cross sections for OH(v, F_1, $j = {}^3/_2$) + H → OH(v', F_1, j') + H for the collision energy of 580.3 cm^{-1} for the three relaxation processes.

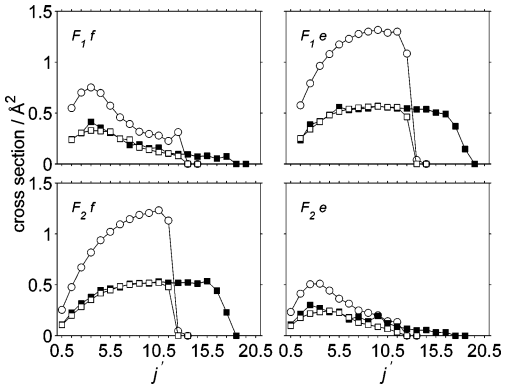

Figure 9. State-to-state OH(v, F_1, $j = {}^3/2$) + H → OH(v', F_i', j', e') + H cross sections at a collision energy of 12 cm^{-1}. As in Figure 8 the open circles, filled squares, and open squares designate respectively $v = 1 \rightarrow 0$, $v = 2 \rightarrow 0$ and $v = 2 \rightarrow 1$ processes.

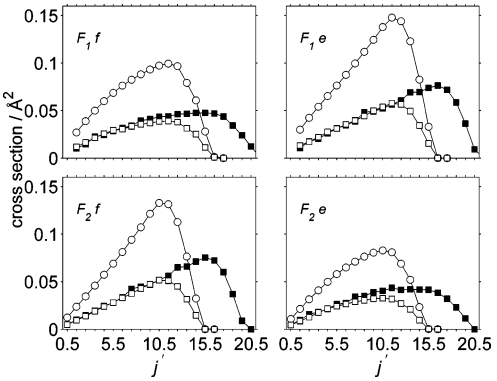

Figure 10. State-to-state OH(v, F_1, $j = {}^3/_2$) + H → OH(v', F_i', j', ϵ') + H cross sections at a collision energy of 1520.3 cm^{-1}. As in Figure 8 the open circles, filled squares, and open squares designate respectively $v = 1 \rightarrow 0$, $v = 2 \rightarrow 0$ and $v = 2 \rightarrow 1$ processes.

Consequently, it is clear that complex-mediated vibrational relaxation results in very different propensity rules than direct relaxation. As discussed earlier, and seen in Figure 5, for direct processes, simple SSH theory[54,55] predicts much larger cross sections for $v \rightarrow v - 1$ as compared to $v \rightarrow v - 2$ transitions, and furthermore, that the cross sections for $v \rightarrow v - 1$ transitions will increase as a function of the initial vibrational quantum number.

3.3. Final State Populations. Figures 9 and 10 show the dependence on the final rotational, spin−orbit, and Λ-doublet state of the cross sections for $v = 2 \rightarrow 1$, 0 and $v = 1 \rightarrow 0$ relaxation at both very low and high collision energies (E_c = 12 and 1520 cm^{-1}). We observe that relaxation to the Π(A′) levels exhibits the "prior" like dependence on the final rotational quantum number,[21,23,59,60] expected for a statistical mechanism. However, at $E_c = 12$ cm^{-1} (and, in fact, at all collision energies below ≈800 cm^{-1}) the cross section for production of OH products in the Π(A″) rotational levels are smaller in magnitude and do not display a similar "prior"-like shape. As discussed in our earlier paper on the O(^{1}D) + H$_2$→OH + H reaction,[23] decay of the HOH complex leads preferentially to OH products in the Π(A′) Λ-doublet levels. Production of the Π(A″) Λ-doublet levels are a result of curve crossing as the OH−H fragments recede.

Further, in our earlier study[23] of the O + H$_2$ → OH + H reaction, we observed that the OH products in Π(A′) Λ-doublet levels were produced with a significantly larger degree of rotational excitation than the products in the Π(A″) Λ-doublet levels. This is exactly what is seen here. As we might have anticipated, the rotational and Λ-doublet distributions are very similar for OH produced from reaction or by vibrational relaxation. Within a statistical model, at a given total energy the decay of the HOH complex will give identical product distributions, regardless of whether the complex is formed by the O(^{1}D) + H$_2$ reaction or by collision of vibrationally excited OH with H.

We observe in Figure 10 that at higher initial collision energy the propensity toward production of products in the Π(A′) Λ-doublet levels is still present, although less pronounced. In addition, at this higher energy the product rotational distributions associated with both Λ-doublet levels show a "prior"-like shape.

3.4. Vibrational Relaxation Rate Constants. If we assume a Maxwellian distribution of translational energy at temperature T, the thermal rate constant is given by[62]

$$k_{i\rightarrow f}(T) = \langle v\sigma_{i\rightarrow f}\rangle = \left[\frac{8}{\pi\mu(kT)^3}\right]^{1/2}\int_0^\infty E_c\sigma_{i\rightarrow f}(E_c)\exp\left(-\frac{E_c}{kT}\right)\mathrm{d}E_c \quad (24)$$

where v is the initial relative velocity and E_c is the initial translational energy (collision energy), for the OH reactant in initial state i. Here, the indices i and f designate the full set of initial and final quantum numbers $\{vjF_i\epsilon\}$. The overall thermal rate constant, for the OH reactant in initial state i, is obtained by summing over all energetically accessible product states, namely

$$k_i(T) = \sum_f k_{i\rightarrow f}(T) \quad (25)$$

The overall thermally averaged rate constant for the title reaction is then obtained by averaging over an assumed Boltzmann distribution of OH rotational levels,

$$k(T) = \frac{\sum_i g_i \exp(-\epsilon_i/kT)k_i(T)}{Q} \quad (26)$$

Here $Q(T)$ is the partition function and g_i and ϵ_i designate, respectively, the degeneracy and internal energy of the ith state of the OH reactant. The sum in eq 26 runs over both spin−orbit manifolds.

Figure 11 shows the temperature dependence of the thermally averaged $v = 1 \rightarrow 0$ vibrational relaxation rate constant. The experimental values[26] of the room temperature $v = 1 \rightarrow 0$ rate constant are also shown. In the experiment, vibrationally excited OH is produced by photolysis of water, itself initially vibrationally excited. We assume that rotational relaxation of the

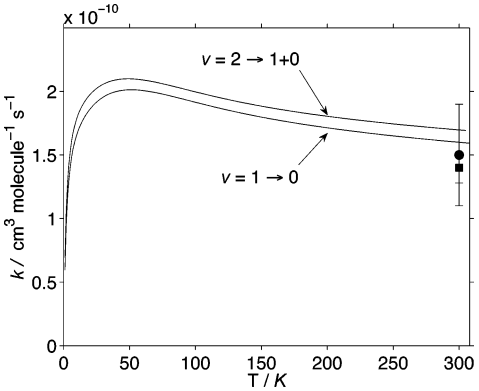

Figure 11. Comparison of thermally averaged vibrational removal rate constants for OH(v = 1, 2) + H. The experimental v = 1 room temperature value is from ref 26. The filled circle and filled square designate rate constants derived from experiments in which H_2O was excited respectively to the |13⟩ or |12⟩ vibrational level before photolysis.

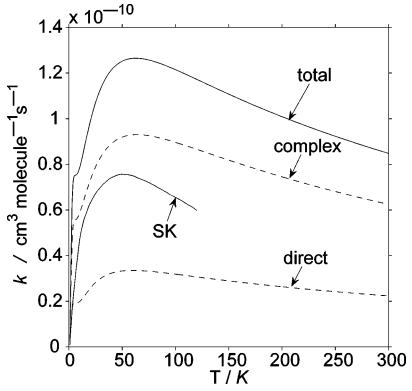

Figure 12. State-to-state thermal rate constant for the transition between the two Λ-doublet levels of the ground rotational level (j = $^3/_2$, F_1).

nascent OH photolysis products will be rapid compared to vibrational relaxation, so that a comparison can be made with our thermally averaged rate constants. The agreement between our calculated $v = 1 \rightarrow 0$ rate constant and the earlier experimental values[26] is excellent. We see from Table 1 that the earlier calculations of Quack and Troe[16] predict room-temperature vibrational relaxation rate constants which are somewhat higher.

Figure 11 also compares the temperature dependence of the thermally averaged rate constants for vibrational removal (deactivation) of the $v = 1$ and $v = 2$ vibrational levels. The latter includes both the $v = 2 \rightarrow 1$ and $v = 2 \rightarrow 0$ processes. In atmospheric modeling, this vibrational removal rate constant is an important parameter.[13] We observe that the total vibrational removal rate for the $v = 2$ manifold is slightly larger than that for $v = 1$. The temperature dependence of the two vibrational removal rates is, however, very similar. In answer, then, to the question raised in the Introduction, we predict, at least for the $v = 1$ and $v = 2$ levels, that the overall vibrational removal rate will depend but little on the initial vibrational quantum number.

3.5. Rotational Excitation and Λ-Doublet Inversion. As mentioned in the Introduction, the importance of the OH astronomical maser has stimulated considerable discussion about the role of rotationally inelastic collisions in either producing or destroying the population inversion that is responsible for maser emission.[31−34] In an attempt to investigate collisional pumping mechanisms, some 25 years ago Shapiro and Kaplan (SK) presented theoretical calculations of rotational excitation rate constants for the OH + H systems.[41] These calculations were based on earlier ab initio potential energy surfaces for the $^1A'$ and $^3A''$ states. Shapiro and Kaplan made additional approximations for the potential surfaces for the $^3A'$ and $^1A''$ states, which were not then available. Cross sections were obtained within the exponential Born approximation. These limitations, both in the treatment of the dynamics and in the description of the potential energy surfaces, can now be overcome. With the availability of high-quality ab initio potential energy surfaces for all four OHH states,[23] we present here the results of coupled-states statistical calculations for rotational excitation of OH($v = 0$) for 1.5 cm $^{-1} < E_c < 795$ cm^{-1}.

Our formulation of the OH + H system does not include the nuclear spin quantum number, $\mathcal{I}$. For comparison, then, we sum and average the hyperfine-resolved rate constants reported by Shapiro and Kaplan over the nuclear spin quantum number:

$$k_{jF_1\epsilon\rightarrow j'F'\epsilon'} = \frac{1}{2}\sum_{\mathcal{I}\mathcal{I}'} k_{jF_1\epsilon\mathcal{I}\rightarrow j'F'\epsilon'\mathcal{I}'} \tag{27}$$

We then compare these rate constants with those from the present calculations, summed and averaged over the H-atom spin-states, namely

$$k_{jF_1\epsilon\rightarrow j'F'\epsilon'} = \frac{1}{2}\sum_{\sigma_h\sigma_h'} k_{jF_1\epsilon\sigma_h\rightarrow j'F'\epsilon'\sigma_h'} \tag{28}$$

At low temperature, the largest relaxation rate constant is associated with Λ-doublet changing transitions within a given rotational level. It is these processes that lead to thermalization of a nonequilibrium Λ-doublet population. The temperature dependence of the rate constant for the Λ-doublet changing transition within the lowest (j = $^3/_2$, F_1) level is shown in Figure 12. In contrast to the case of vibrational relaxation, discussed earlier in this paper, the direct and capture processes make a roughly equal contribution here.

Despite the approximations made by Shapiro and Kaplan to both the OH + H potential energy surfaces and in their treatment of the scattering dynamics, we observe that the magnitude and temperature dependence of their calculated rate constant agrees reasonably well with our present calculation. Within the interstellar cloud model they adopted, Shapiro and Kaplan concluded that for most reasonable H-atom densities even a collisional rate on the order of 10^{-10} cm^3 molecule^{-1} s^{-1} is not large enough to thermalize effectively a nonequilibrium Λ-doublet population in the j = $^3/_2$, F_1 level.

Figure 13 shows the temperature dependence of the four possible $\epsilon \rightarrow \epsilon'$ transitions corresponding to j = $^3/_2 \rightarrow {}^5/_2$ rotational excitation in the lower (F_1) spin−orbit manifold. We observe a large difference between the rate constants for the ϵ-changing as compared to ϵ-conserving transitions. As seen in the figure, the much larger contribution of direct scattering to the ϵ-changing transitions results in a larger total rate constant. This ϵ, ϵ' propensity seen in the rate constants—and in the underlying cross sections (not shown)—is entirely similar to the propensities seen earlier in collisions of molecules in $^2\Pi$ electronic states with closed-shell atomic collision partners.[63−65] These propensities are a reflection of the contribution of different components in the anisotropy in the potential energy surface to the coupling between two levels of the same ($e \rightarrow e$ or $f \rightarrow f$) as opposed to opposite ($e/f \rightarrow f/e$) symmetry index.

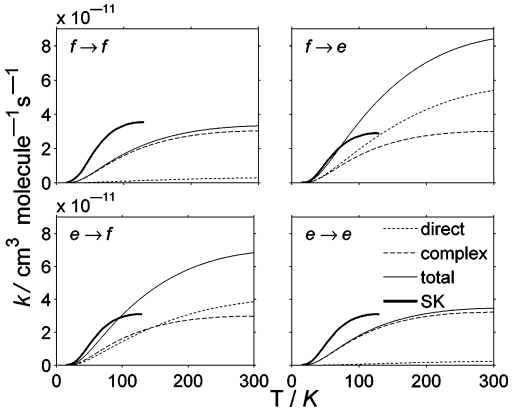

Figure 13. State-to-state direct, complex-mediated and total rate constants for the OH($j = {}^3/_2$, F_1, ϵ) + H → OH($j' = {}^5/_2$, F_1, ϵ') transition within the $v = 0$ manifold. The heavy solid curves depict the results of Shapiro and Kaplan.[41]

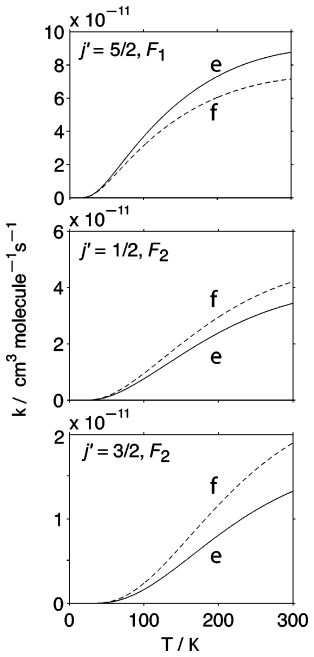

Figure 14. Initial *e*/*f*-averaged rate constants for transitions out of the OH($v = 0$, F_1, $j = {}^3/_2$) level into both Λ-doublet levels for $j' = {}^5/_2$, F_1, $j' = {}^1/_2$, F_2 and $j' = {}^3/_2$, F_2.

We also observe in Figure 13 that the degree of variation of the rotational excitation cross section with the *e*/*f* index predicted by the present calculations is much larger than predicted by the earlier calculations of Shapiro and Kaplan.[41] In addition, the rate constants determined by Shapiro and Kaplan predict, in direct contrast to the present calculations, that the *e*/*f* conserving transitions will be more efficient than the *e*/*f* changing transitions.

In comparison with the direct contributions, the complex-mediated contributions to the cross sections (not shown) and rate constants (Figure 13) are virtually insensitive to the initial and final Λ-doublet indices. The capture cross sections are largely determined by the overall topology of the attractive ^{1}A′ potential energy surface. Any variation with ϵ of the capture cross sections for a particular jF_i will reflect the differing degree to which the *e* and *f* Λ-doublet states will access the ^{1}A′ potential energy surface. This difference is likely to be small.

Figure 14 plots the rate constants for collisional excitation from the $j = {}^3/_2$, F_1 level (with an assumed equal population in the two Λ -doublets), to the next rotational level ($j = {}^5/_2$) in the lower (F_1) spin−orbit manifold as well as into the $j = {}^1/_2$ and $j = {}^3/_2$ levels of the higher (F_2) spin−orbit manifold. We observe, referring back to Figure 3, that collisional excitation will not lead to population inversion in the former case but will lead to population inversion in the spin−orbit changing processes. The calculated *e*/*f* collisional propensity supports the proposed maser-pumping mechanism mentioned in the Introduction,[31−34,36,66] whereby if collisional excitation populates preferentially the upper Λ-doublet, then subsequent radiative transitions to the ground rotational level, which by necessity change the parity but conserve the Λ-doublet label, will provide a pump mechanism for the maser. However, for collisions of OH with molecular hydrogen (H_2) the most recent,[39] as well as earlier,[36] calculations predict, in contrast to the present calculations (OH + H), that collisions out of the $j = {}^3/_2$, F_1 level, averaged over both initial Λ-doublets, will not result in a population inversion in the lower rotational levels of the F_2 spin−orbit manifold.

4. Summary

We have performed a close-coupled, statistical study of vibrational and rotational relaxation of OH($^2\Pi$) in collisions with H atoms. The method and Hamiltonian include all couplings exactly in the long-range part of the potential but treat formation and decay of the HOH complex region statistically. Our calculations allow us to separate the contributions to vibrational and rotational relaxation due to inelastic scattering involving both the repulsive regions of the ^{1}A′ potential energy surface as well as coupling between the ^{1}A′ potential energy surface and the repulsive ^{1}A″, ^{3}A′, and ^{3}A″ potential energy surfaces from processes which enter the HOH complex and then reemerge into different internal states of the OH moiety. We found that the direct and complex-mediated mechanisms make comparable contributions to rotationally inelastic processes. However, for vibrationally inelastic processes, where the direct contribution is extremely small, the complex-mediated contribution remains large. Thus, as Smith has suggested,[7] vibrational relaxation in radical−radical encounters by means of complex-forming collisions can be a far more efficient process than in the case of closed-shell collision partners. Further, because complex-forming processes dominate, it may well be that statistical method calculations which incorporate only the lowest (^{1}A′) potential-energy-surface will yield accurate vibrational removal rate constants.

At 300 K, the total rate constant for removal from OH($v = 2$) (1.697×10^{-11} cm^3 molecule^{-1} s^{-1}) is slightly higher than for removal from OH($v = 1$) (1.600 in the same units). The $v = 1$ calculated removal rate constant agrees extremely well with earlier experimental measurements from the Smith group[26] but is somewhat smaller than the earlier predictions of Quack and Troe.[16]

Because the complex-mediated mechanism dominates, our calculations also predict that vibrational relaxation will lead to rotationally hot OH products. In addition, and entirely similar to our earlier study of OH produced by the O(^{1}D) + H_2 reaction,[23] we predict that the relaxed OH will be found preferentially in the Π(A′) Λ-doublet level. Observations of atmospheric OH, produced in reactions 1 and 2, show a markedly larger population in the Π(A′) Λ-doublet levels.[13] Although collisions with H may not play a major role in the vibrational relaxation of OH in the mesosphere, the results of the present study certainly suggest that complex-mediated vibrational relaxation, through collisions with other radicals (possibly O atoms), could well result in the observed inequalities in the Λ-doublet populations.

Our calculations also predict that, at least for relaxation of OH due to collisions with H, the vibrational removal rate will be insensitive to the initial vibrational quantum number, in contrast to the predictions of SSH theory.

We also investigated rotationally inelastic collisions in the $v = 0$ manifold as a possible contributor to population inversion within the Λ-doublet of the lowest ($j = {}^3/_2$, F_1) rotational level of OH in interstellar gas clouds. Our calculations, which are free of the approximations which limited the much earlier work of Shapiro and Kaplan,[41] suggest that collisional excitation to the upper spin−orbit manifold, F_2, followed by radiative relaxation to the ground rotational level in the F_1 manifold, will lead to this population inversion. Along with the considerable body of theoretical work on rotationally inelastic collisions of OH with H_2,[35−37,39,40] the present calculations on collisions of OH with H should provide insight and input into modeling of the pump mechanism of the OH maser in astronomical environments, where both OH and H are both abundant. This can occur, for example, in dense molecular clouds that are subject to fast interstellar shock waves.[67]

Acknowledgment. We are grateful to the U.S. Air Force Office of Scientific Research for support of this research under grant FA9550-04-1-0152. We also thank Professors Ian Smith, Paul Dagdigian, and David Neufeld for helpful discussions. It is a pleasure to contribute this article to a volume honoring the career and contributions of John Light. His pioneering work on statistical models in chemical kinetics is still of great relevance.

References and Notes

(1) Meriwether, J. W. *J. Geophys. Res.* **1989**, *94*, 14629.
(2) Berresheim, H.; Plass-Dulmer, C.; Elste, T.; Mihalopoulos, N.; Rohrer, F. *Atmos. Chem. Phys.* **2003**, *3*, 639.
(3) Dodd, J. A.; Lipson, S. J.; Lowell, J. R.; Armstrong, P. S.; Blumberg, W. A. M.; Nadile, R. M.; Adler-Golden, S. M.; Marinelli, W. J.; Holtzclaw, K. W.; Green, B. D. *J. Geophys. Res.-Atmos.* **1994**, *99*, 3559.
(4) Chalamala, B. R.; Copeland, R. A. *J. Chem. Phys.* **1993**, *99*, 5807.
(5) Sappey, A. D.; Copeland, R. A. *J. Chem. Phys.* **1990**, *93*, 5741.
(6) Glass, G. P.; Endo, H.; Chaturvedi, B. K. *J. Chem. Phys.* **1982**, *77*, 5450.
(7) Smith, I. W.; Williams, M. D. *J. Chem. Soc., Faraday. Trans. 2.* **1985**, *81*, 1849.
(8) Brunning, J.; Derbyshire, D. W.; Smith, I. W. M.; Williams, M. D. *J. Chem. Soc., Faraday. Trans. 2* **1988**, *84*, 105.
(9) Rensberger, K. J.; Jeffries, J. B.; Crosley, D. R. *J. Chem. Phys.* **1989**, *90*, 2174.
(10) Dodd, J. A.; Lipson, S. J.; Blumberg, W. A. M. *J. Chem. Phys.* **1991**, *95*, 5752.
(11) Knutsen, K.; Dyer, M. J.; Copeland, R. A. *J. Chem. Phys.* **1996**, *104*, 5798.
(12) Dyer, M. J.; Knutsen, K.; Copeland, R. A. *J. Chem. Phys.* **1997**, *107*, 7809.
(13) Holtzclaw, K. W.; Upschulte, B. L.; Caledonia, G. E.; Cronin, J. F.; Green, B. D.; Lipson, S. J.; Blumberg, W. A. M.; Dodd, J. A. *J. Geophys. Res-Space Phys.* **1997**, *102*, 4521.
(14) Lacoursiere, J.; Dyer, M. J.; Copeland, R. A. *J. Chem. Phys.* **2003**, *118*, 1661.
(15) Spencer, J. E.; Glass, G. P. *Chem. Phys.* **1976**, *15*, 35.
(16) Quack, M.; Troe, J. *Ber. Bunsen-Ges. Phys. Chem. Chem. Phys.* **1977**, *81*, 160.
(17) Quack, M.; Troe, J. *Ber. Bunsen-Ges. Phys. Chem.* **1975**, *79*, 170.
(18) Quack, M.; Troe, J. In *Encyclopedia of Computational Chemistry*; von Rague Schleyer, P., Allinger, N., Clark, T., Gasteiger, J., Kollmann, P. A., Schaefer, H. F., Eds.; Wiley: New York, 1998; Vol. 4, p 2708.
(19) Nikitin, E. E.; Umanski, S. Y. *Faraday Discuss. Chem. Soc.* **1972**, *53*, 7.
(20) Alexander, M. H. *Chem. Phys.* **1985**, *92*, 337.
(21) Rackham, E. J.; Huarte-Larrañaga, F.; Manolopoulos, D. E. *Chem. Phys. Lett.* **2001**, *343*, 356.
(22) Rackham, E. J.; Gonzalez-Lezaña, T.; Manolopoulos, D. E. *J. Chem. Phys.* **2003**, *119*, 12895.
(23) Alexander, M. H.; Rackham, E. J.; Manolopoulos, D. E. *J. Chem. Phys.* **2004**, *121*, 5221.
(24) Lin, S. Y.; Guo, H. *J. Chem. Phys.* **2004**, *120*, 9907.
(25) Lin, S. Y.; Guo, H. *J. Phys. Chem. A* **2004**, *108*, 10066.
(26) Barnes, P. W.; Sharkey, P.; Sims, I. R.; Smith, I. W. M. *Faraday Discuss.* **1999**, *113*, 167.
(27) Pavlakis, K.; Kylafis, N. *Astrophys. J.* **1996**, *467*, 300.
(28) A. L. Argon, M. J. R.; Menten, K. M. *Astrophys. J. Suppl. S.* **2000**, *129*, 159.
(29) Wardle, M.; Yusef-Zadeh, F. *Science* **2002**, *296*, 2350.
(30) Dousmanis, G. C.; Sanders, T. M.; Townes, C. H. *Phys. Rev.* **1955**, *100*, 1735.
(31) Litvak, M. M. *Science* **1969**, *165*, 855.
(32) Gwinn, W. D.; Turner, B. E.; Goss, W. M.; Blackman, G. L. *Astrophys. J.* **1973**, *179*, 789.
(33) Bertojo, M.; Cheung, A. C.; Townes, C. H. *Astrophys. J.* **1976**, *208*, 914.
(34) Andresen, P. W. *Astron. Astrophys.* **1986**, *154*, 42.
(35) Dewangan, D.; Flower, D. *J. Phys. B.: At. Mol. Phys* **1981**, *14*, L425.
(36) Schinke, R.; Andresen, P. *J. Chem. Phys.* **1984**, *81*, 5644.
(37) Corey, G. C.; Alexander, M. H. *J. Chem. Phys.* **1988**, *88*, 6931.
(38) Miller, S. M.; Clary, D. C.; Kliesch, A.; Werner, H.-J. *Mol. Phys.* **1994**, *83*, 405.
(39) Offer, A. R.; van Hemert, M. C.; van Dishoeck, E. F. *J. Chem. Phys.* **1994**, *100*, 362.
(40) Schreel, K.; ter Meulen, J. J. *J. Chem. Phys.* **1996**, *105*, 4522.
(41) Shapiro, M.; Kaplan, H. *J. Chem. Phys.* **1979**, *71*, 2182.
(42) Honvault, P.; Launay, J.-M. *J. Chem. Phys.* **2001**, *114*, 1057.
(43) Pechukas, P.; Light, J. C. *J. Chem. Phys.* **1965**, *42*, 3281.
(44) Nikitin, E. E. *J. Chem. Phys.* **1965**, *43*, 744.
(45) Clary, D. C.; Henshaw, J. P. *Faraday Discuss. Chem. Soc.* **1987**, *84*, 333.
(46) Pechukas, P.; Light, J. C.; Rankin, C. *J. Chem. Phys.* **1966**, *44*, 794.
(47) Lefebvre-Brion, H.; Field, R. *Perturbations in the Spectra of Diatomic Molecules*; Academic: New York, 1986.
(48) Alexander, M. H. et al. *J. Chem. Phys.* **1988**, *89*, 1749.
(49) Brown, J. M.; Hougen, J. T.; Huber, K.-P.; Johns, J. W. C.; Kopp, I.; Lefebvre-Brion, H.; Merer, A. J.; Ramsay, D. A.; Rostas, J.; Zare, R. N. *J. Mol. Spectrosc.* **1975**, *55*, 500.
(50) Nikitin, E. E.; Zare, R. N. *Mol. Phys.* **1994**, *82*, 85.
(51) Secrest, D. In *Atom-Molecule Collision Theory: A Guide for the Experimentalist*; Bernstein, R., Ed.; Plenum: New York, 1979.
(52) Manolopoulos, D. C. *J. Chem. Phys.* **1986**, *85*, 6425.
(53) Alexander, M. H.; Manolopoulos, D. E. *J. Chem. Phys.* **1987**, *86*, 2044.
(54) R. N. Schwartz, Z. I. Slawsky, K. H. *J. Chem. Phys.* **1952**, *20*, 1591.
(55) Lambert, J. D. *Vibrational and Rotational Relaxation In Gases*; Clarendon Press: Oxford, U.K., 1977.
(56) Krems, R. V.; Nordholm, S. *J. Chem. Phys.* **2001**, *115*, 10581.
(57) R. V. Krems, A. A. Buchachenko, N. M.; Nordholm, S. *J. Chem. Phys.* **2002**, *117*, 166.
(58) Clary, D. C.; Werner, H.-J. *Chem. Phys. Lett.* **1984**, *112*, 346.
(59) Atahan, S.; Alexander, M. H.; Rackham, D. E. Unpublished data.
(60) Levine, R. D.; Bernstein, R. B. *Molecular Reaction Dynamics*, 1st ed.; Oxford: Oxford, U.K., 1974.
(61) Huber, K. P.; Herzberg, G. *Molecular Spectra and Molecular Structure. IV. Constants of Diatomic Molecules*; Van Nostrand Reinhold: New York, 1979.
(62) Smith, I. W. M. *Kinetics and dynamics of elementary gas reactions*; Butterworth: London, 1980.
(63) Dagdigian, P. J.; Alexander, M. H.; Liu, K. *J. Chem. Phys.* **1989**, *91*, 839.
(64) Alexander, M. H.; Dagdigian, P. J. *J. Chem. Phys.* **1994**, *101*, 7468.
(65) Dagdigian, P. J. *Annu. Rev. Phys. Chem.* **1997**, *48*, 123.
(66) Andresen, P.; Häusler, D.; Lülf, H.; Kegel, W. *Astron. Astrophys.* **1984**, *138*, L17.
(67) Neufeld, D.; Dalgarno, A. *Astrophys. J.* **1989**, *340*, 869.